Batteries & Supercaps

Research Article
doi.org/10.1002/batt.202300176

Chemistry Europe
European Chemical Societies Publishing

www.batteries-supercaps.org

Special Collection

Tuning Polybenzimidazole-Derived Crosslinked Interpenetrating Network Membranes for Vanadium Redox Flow Batteries

Alexandros Pasadakis-Kavounis,[a] Funda Arslan,[b] Mads Radmer Almind,[a] David Aili,*[a] and Johan Hjelm*[a]

Non-fluorinated ion exchange membranes with high proton selectivity and conductivity are sought as separators for vanadium redox flow batteries (VRFB) to substitute the typically used perfluorosulfonic acid (PFSA) polymer membranes. Polybenzimidazole based membranes offer a promising non-fluorinated alternative due to their excellent thermomechanical properties, low vanadium crossover, and ionic conductivity in acidic media. In this work, a series of polybenzimidazole-polyvinylchloride polymer blends were cast and decorated with different quaternary ammonium functionalities. The polymer blends were systematically studied with respect to the blend composition and chemical structure of the quaternary ammonium groups. Assessment of relevant membrane properties for use in an aqueous acidic flow battery was conducted through a combination of VRFB single cell testing, permeability measurements, water/electrolyte uptake, and infrared spectroscopy. The blend with a polybenzimidazole content of 90% decorated with DABCO (1,4-diazabicyclo[2.2.2]octane) was found to combine low polarization resistance with low swelling and high stability. The performance was found to be similar to that of a benchmark polybenzimidazole membrane despite being three times thicker. This led to the conclusion that quaternary ammonium functionalized polybenzimidazole-polyvinylbenzylchloride systems is an excellent candidate for further modification or fabrication of thinner membranes to further reduce the membrane resistance without compromising on vanadium blocking properties.

Introduction

Energy storage for grid balancing has been identified as a major component of expanding renewable energy systems with a high share of wind and solar.[1] Electrochemical energy storage in the form of redox flow batteries can deliver the capacity needed to regulate the intermittent energy production of renewables.[2] Their independent scalability of energy and power alongside expected lifetimes of over 10 years are very attractive features for large scale energy storage.[2] Additionally, RFBs can deliver energy during high demand and store energy during low demand, making obsolete the need of installing extra generating capacity.[2] Various aqueous and non-aqueous redox chemistries have been explored within redox flow batteries, and systems based on aqueous vanadium electrolytes is the frontrunner and have developed to a relatively technologically mature stage.[3]

Vanadium redox flow batteries (VRFB) rely on the four different oxidation states of vanadium to deliver the desired potential. The negative and positive side of a typical VRFB consist of aqueous sulfuric acid solutions of V^{2+}/V^{3+} and VO^{2+}/VO_2^{+}, respectively.[4] The concentration of vanadium is at around 2 mol L^{-1} due to solubility limitations.[5] An ion exchange membrane (IEM) separates the two compartments with the main function to block crossover of cationic vanadium species, while supporting high proton conductivity.[6] Additionally it should be chemically and mechanically stable and have low cost.[7]

The redox-active vanadium species and hydrated protons are both positively charged, which means that the selectivity of the IEM needs to be controlled by means of size sieving.[8] Perfluorosulfonic acid (PFSA) membranes currently used for proton transport suffer from high cost and crossover of the positively charged vanadium ions.[2,4] The low selectivity of PFSA membranes is due to the relatively large dimensions of the aqueous domains within the PFSA membrane, which far exceed dimensions of the cationic vanadium ions. Therefore, the ionic size-sieving characteristics of PFSA membranes are insufficient to allow for fast and selective proton conduction.

Polybenzimidazole (PBI) is a large group of polymers containing benzimidazole units as a part of the backbone. In

[a] A. Pasadakis-Kavounis, Dr. M. Radmer Almind, Dr. D. Aili, Prof. J. Hjelm
Department of Energy Conversion and Storage
Technical University of Denmark
Fysikvej, Building 310, 2800 Kgs. Lyngby (Denmark)
E-mail: larda@dtu.dk
johh@dtu.dk

[b] Dr. F. Arslan
Forschungszentrum Jülich GmbH
Helmholtz Institute Erlangen-Nürnberg for Renewable Energy (IEK-11)
91058 Erlangen (Germany)

Supporting information for this article is available on the WWW under https://doi.org/10.1002/batt.202300176

Special Collection An invited contribution to a Special Collection dedicated to NordBatt 2022 conference.

the fully aromatic form, these polymers have excellent thermomechanical properties and chemical stability.[9] Additionally, due to their ion conducting properties when combined with Brønsted acids or bases, PBI membranes have been explored for use in electrochemical systems, such as flow batteries, fuel cells, electrolysers.[10] Sulfuric acid, which is the main component in the electrolyte used in VRFB at a concentration of approximately 2 mol L^{-1}, is sufficiently acidic to nearly completely protonate the benzimidazole units along the polymer backbone. This results in a protic cationic polymeric salt with associated bisulfate anions that balance the positive charge. Electrostatic charge repulsion by Donnan exclusion could, at least partly, explain the low vanadium cation permeability of PBI membranes in acidic environment as discussed by Noh et al.[11] However, in high ionic strength solutions, the situation is more complex because the Donnan exclusion effect diminishes as the volume fraction of electrolyte within the membrane increases. With increasing electrolyte uptake, the partial conductivities of the different ionic species within the aqueous domain of the membrane approaches that of the pure aqueous solution. However, steric effects must also be considered when the dimensions of the ionic pathways through the membrane are on the same length scale as the dimensions of the hydrated ions.[12] As recently discussed by Wang et al.[8], engineered membranes with <7 Å ionic domains are a rational strategy for suppressing vanadium crossover while maintaining high proton conductivity. This membrane design based on sulfonated poly(arylene alkylene)s allowed for smaller hydrated cations, such as protons, to pass through at small ohmic losses while larger cations, such as vanadium cations, were effectively blocked.

The development of PBI membrane for VRFB applications has focused on exploration of different backbone chemistries,[7,11,13] pretreatment methods,[4,14] polymer blends,[15–18] and post-functionalization strategies[19–21] to balance ionic conductivity and undesired crossover. As reviewed by Chen et al.[22] the area-specific resistance, permeability and energy efficiency are parameters that can be tuned by modifying the chemical structure and composition of the membrane. Most of the modified PBI membranes reported have an area specific resistance from 0.2 $\Omega\,cm^2$ to 0.5 $\Omega\,cm^2$ with some notable exceptions. Jang et al.[7] grafted alkyl groups levels on AB-PBI by *N*-coupling at different grafting. Because the alkyl groups act as spacers, the morphology of the polymer is more amorphous, which increases the electrolyte uptake. It resulted in an area resistance of only 0.06 $\Omega\,cm^2$ after equilibration in the aqueous electrolyte, and a vanadium permeability of 9.78×10^{-8} $cm^2\,min^{-1}$, approximately one order of magnitude lower than Nafion 115 ($5.2\times10^{-7}\,cm^2\,min^{-1}$). Crosslinking of PBI with other hydrophobic macromolecules can yield membranes with good mechanical properties and tunable ionic channels for selective transportation of protons. Crosslinking can either be achieved covalently,[17] or ionically.[16,18,23] However, it has been shown that the latter results in reduced ionic conductivity as the crosslinking occupies basic sites on PBI, decreasing the electrolyte uptake.[22]

Noh et al. have shown that decreasing the thickness of poly(2,2′-(*m*-phenylene)-5,5′-bibenzimidazole) (mPBI) results in higher voltage- and coulombic efficiency.[11] A higher voltage efficiency is expected by reducing the thickness, as this results in a decrease of the ohmic resistance of the membrane. The area specific resistance increased from 1.62 $\Omega\,cm^2$ for 15 μm thickness mPBI to 2.03 $\Omega\,cm^2$ when the thickness was increased to 35 μm.[11] Thicker membranes should intuitively have better barrier properties for vanadium crossover; however, the authors observed that coulombic efficiency decreased with increasing thickness. The decreased coulombic efficiency was hypothesized to stem from the higher potential required during the charging step. The result of that could be either more hydrogen evolution and/or a larger portion of vanadium ions overcoming the energy barrier necessary to transfer through the membrane.[11]

Herein, we report the use of poly[2,2′-(4,4′-oxybis(1,4-phenylene))-5,5′-bibenzimidazole] (OPBI) membranes crosslinked with poly(vinylbenzyl chloride) (PVBC) and functionalized with a series of quaternary ammonium groups for use in VRFB. The polymer blend system has previously been tested in high temperature polymer electrolyte fuel cells (HT-PEMFS) in combination with phosphoric acid doping.[24] It was found to combine high electrolyte uptake with relatively low volume swelling and good mechanical characteristics, which are attractive characteristics in the VRFB context. As such, different ratios of OPBI/PVBCl were prepared, characterized, and tested in 1.6 M vanadium solution by means of electrochemical impedance spectroscopy (EIS), polarization behavior, vanadium permeability and charge/discharge cycling.

Experimental Section

Membrane materials and preparation

The OPBI was purchased from Fumatech BWT GmbH. Poly(vinylbenzyl chloride) (PVBC) was purchased from Scientific Polymer Products. 1,4-Diazabicyclo(2.2.2)octane (DABCO) and 85 wt % ortho-phosphoric acid (PA) were obtained from Merck. 1-Azabicyclo(2.2.2)octan-3-ol (quinuclidinol, QOL) and 1-azabicyclo(2.2.2)octane (quinuclidine, QINE) were purchased from Sigma-Aldrich and Alfa Aesar, respectively. All chemicals were used as received.

The membranes were prepared following procedures described in the literature.[24] In brief, 5 wt% OPBI and 15 wt% PVBC solutions were prepared by dissolving the polymers in dimethyl sulfoxide (DMSO). The OPBI solution was stirred overnight at 50 °C, and the PVBC solution was stirred for 1 h at room temperature. Subsequently, the solutions were blended to yield the weight ratios OPBI: PVBC of 60:40, 75:25, and 90:10. Before casting onto a glass plate, the blend solutions were stirred for 30 min at room temperature until a homogenous solution was obtained. Casting was performed using an automated film applicator (ZAA 2300, Zehntner) with a blade length of 8 cm and a speed of 20 $mm\,s^{-1}$. Membranes were formed by solvent evaporation for 24 h at 80 °C, followed by 5 h under reduced pressure at the same temperature.

The electrolyte solution used for battery testing and electrolyte uptake consisted of 1.6 M V^{3+}/V^{4+} (50:50) dissolved in 2.4 M H_2SO_4 with 0.05 M H_3PO_4. The total sulfate content in this electrolyte was

4 M. The solution used for vanadium crossover measurements was 1 M vanadyl sulfate, $VOSO_4$, (Sigma Aldrich) in 2 M H_2SO_4 (source side) on one side, and 1 M $MgSO_4$ in 2 M H_2SO_4 (receiver side) in the other.

For quaternization, the membranes were immersed in 0.5 M solutions of the three different amines (DABCO, QOL, or QINE) in ethanol for 24 h at 60 °C. Subsequently, the membranes were rinsed with DI water, anion exchanged in a 1 M KOH solution for 24 h at room temperature and thereafter rinsed extensively.

Membrane characterization

Vanadium crossover measurements were performed for a blend membrane with a 60/40 composition, functionalized with different amines. To prevent formation of concentration gradients in the two-compartment cell the electrolytes on either side were stirred continuously. UV-Vis measurements (Shimadzu 3600) of aliquots from the receiver side were collected daily and the concentration of the permeated $VOSO_4$ was calculated using the signal at 760 nm. A linear fit of $\ln(C_s/(C_s-C_r))$ as function of time was used to calculate the diffusion coefficient as shown in Figure S1 (Supporting Information).

Water and electrolyte uptakes were obtained gravimetrically by measuring the weight difference of dry membranes and after immersion in DI H_2O or vanadium battery electrolyte at room temperature for 24, 48, and 72 h. The membranes were dried at 80 °C overnight under vacuum. The weight difference was calculated according to Equation (1), where W_{wet} and W_{dry} are the wet and dry weights, respectively. The membranes were wiped to remove any excess H_2O and electrolyte from the surface prior to determination of W_{wet}.

$$\text{Liquid Uptake} = (W_{wet} - W_{dry})/W_{dry} \times 100\,\% \quad (1)$$

FTIR spectra were acquired with a Perkin Elmer Spectrum Two FTIR, averaging over 16 scans and using a resolution of 1 cm^{-1}. Membranes that had not been tested were measured as prepared. Meanwhile, membranes that had undergone cell testing were first immersed in MiliQ H_2O (18.2 MΩ·cm) for 24 h, then in 0.5 M K_2CO_3 solution for 24 h and finally immersion in DI H_2O for 48 h. They were then dried under vacuum at 80 °C for 24 h.

Thermogravimetric analysis (TGA) was performed on a Netzsch STA 449 F3 instrument. The samples were heated from room temperature up to 700 °C with a rate of 10 °C per minute. The corresponding plots are shown in Figure S2 in the Supporting Information.

Flow battery single cell testing

Single cell testing was carried out using hardware obtained from Fuel Cell Technologies. The single cell test fixture had polymer-carbon composite flow plates with a flow-through flow-field with an active area of 5 cm^2. The cell consisted of a membrane sandwiched between two pieces of 2.5 mm thick carbon felt from SGL Carbon. The electrodes were rendered hydrophilic by heat treatment in air at 400 °C for 24 h prior to testing. Meanwhile, the membranes were treated in 10 M H_2SO_4 for 48 h and then immersed in 4 M H_2SO_4 for at least 48 h before testing. All the membranes that were tested were mechanically robust before and after acid treatment. More detailed in information about the mechanical properties of the membranes can be found in literature.[24] The compression rate was approximately 20 % and was regulated by using Teflon gaskets of 2 mm thickness. The flow rate used was 30 mL min^{-1}. All measurements took place in an Ar filled cabinet to suppress any self-discharge due to the presence of O_2.

The membranes were assessed using single cell testing with 15–20 ml of vanadium electrolyte on either side and the following order of electrochemical experiments. First, EIS spectra were recorded while a 50:50 mixture of V^{+3}/V^{4+} was flowing on both sides (SoC = −50 %) of the cell. Second, the cell was cycled at 40 mA/cm^2 for 10 cycles (cycle time approximately 4 h) followed by a series of cycles at different current densities ranging from 10 mA/cm^2 to 150 mA/cm^2 between potential limits of 0.7 to 1.9 V. Third, polarization curves were recorded from 100 % SoC down to 10 % SoC with 10 % increments. Coulombic, voltage and energy efficiencies were calculated according to Equations (2), (3) and (4), respectively.

$$\text{Coulombic efficiency (CE)} = Q_{dch}/Q_{ch} \quad (2)$$

$$\text{Voltage efficiency (VE)} = \bar{E}_{dch} \,/\, \bar{E}_{ch} \quad (3)$$

$$\text{Energy efficiency (EE)} = \text{CE} \times \text{VE} \quad (4)$$

A Biologic SP-200 potentiostat was used to collect EIS spectra. A frequency range 500 kHz to 100 mHz was used with 12 logarithmically distributed data points per frequency decade and a 5 mV zero-to-peak amplitude. Polarization curves, permeability measurements and charge discharge cycles were all recorded with a Neware battery testing system (CT-4008-5 V6 A).

Results and Discussion

As described previously,[24] the cross-linked interpenetrating network membranes were prepared by co-casting OPBI and PVBC from DMSO to obtain a visually homogeneous and transparent film. The excess chloromethyl groups from the PVBC component were then converted to the corresponding quaternary ammonium functions by a heterogeneous Menshutkin reaction using three different tertiary amines. Similar protocols have been used to prepare anion exchange membranes from PVBC blended with poly(arylene ether ketoncardo)[25] and poly(arylene ether sulfones)[26].

The chemical structure of the membranes can be seen in Figure 1. The vanadium electrolyte solution used contains 2.4 M H_2SO_4, which can be assumed to be fully dissociated to bisulfate and sulfate anions. As such, the positive charge located on the ammonium cations and on the protonated benzimidazole units of the PBI is charge balanced by the sulfate/bisulfate anions. In the acidic vanadium electrolyte solution, DABCO holds two positive charges owing to the presence of a protonated tertiary amine ($pKaH = 8.7$[27]) in addition to the quaternary ammonium ion. Both QINE and QOL each possess a positive charge, with the difference that the latter carries a hydroxyl group. Since the 60/40 OPBI/PVBC membrane has the highest PVBC content, and thus the highest concentration of reactive chloromethyl groups, it likely has the highest degree of crosslinking and the highest degree of functionalization after quaternization.

FTIR spectra of the membrane blends and mPBI are shown in Figure S3. The spectra are consistent with previous work using the same membranes in HT-PEMFCs.[24] No visible band

Research Article
doi.org/10.1002/batt.202300176
Chemistry Europe
European Chemical Societies Publishing

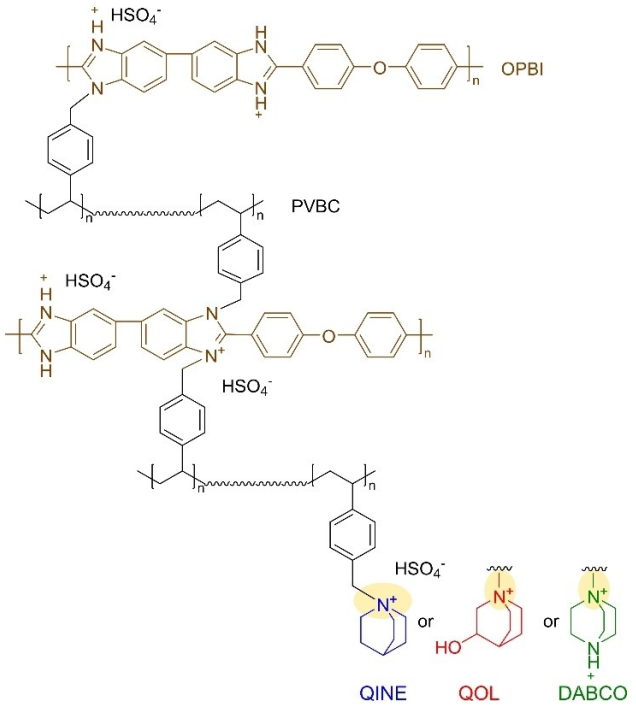

Figure 1. Chemical structures of composite membranes with the three amines used as end groups. The brown polymer chain represents the OPBI while the black polymer represents the PVBC structure in the mixture. The positions where the amines are connected to the polymer backbone are highlighted in yellow.

was observed at 1265 cm^{-1},[28] confirming the complete reaction and quaternization of OPBI/PVBC blend. A more detailed analysis can be found in the supporting information.

The $VOSO_4$ permeability of all three 60/40 blend membranes was very low on the order of 10^{-10} $cm^2 s^{-1}$, whereas Nafion 212 displays a $VOSO_4$ permeability on the order of 10^{-7} $cm^2 s^{-1}$.[29] If the Donnan exclusion effect is the predominant method of blocking vanadium ions, the DABCO membrane should be the most effective because it has the highest number of positively charged groups. However, as mentioned earlier the Donnan exclusion decreases in solutions with high ionic strength, which means that the selectivity is mainly determined by steric effects and the size of hydrophilic channels.[6,8] Among the three tested membranes, the blend membrane decorated with DABCO showed the highest vanadium permeability, while the QOL membranes had the lowest permeability (Figure 2, dark blue bars). Water and electrolyte absorption were found to correlate with the $VOSO_4$ membrane diffusivity as shown in Figure 2 (blue and yellow bars). This supports the hypothesis that the predominant blocking method is size sieving, as DABCO absorbs the most electrolyte and has the highest vanadium permeability among the three.

Coulombic efficiency, energy efficiency, voltage efficiency, polarization resistance and membrane resistance were determined by single-cell tests for each membrane. The three membranes were tested individually to evaluate their performance. An untreated dense 10 µm mPBI membrane was used as a reference. The performance of mPBI can change significantly

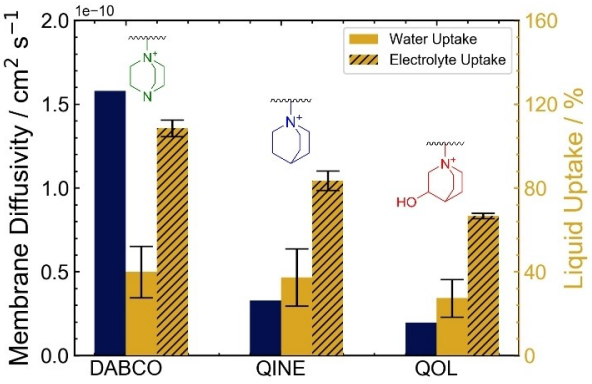

Figure 2. Vanadium diffusivity (dark blue bars, left *y*-axis) of three 40%/60% w/w OPBI-PVBC blends each decorated with different amines, DABCO (green), QINE(blue) and QOL (red). The dark yellow right *y*-axis represent water (dark yellow bars) and electrolyte (dark yellow dashed bars) absorption.

depending on the pretreatment method.[14] For example, the conductivity of dense mPBI pretreated with 2 M H_2SO_4 is below 5 mS cm^{-1} in 2 M H_2SO_4, which increases to 9–12 mS cm^{-1} after pre-treatment in 10 M H_2SO_4 solution.[14]

As can be seen in Figure 3, pre-cycling EIS showed that all three membranes were more conductive than the pristine mPBI membranes. Commonly, conductivity trends are correlated with ion exchange capacity (IEC). In the membranes blends presented in this work, it is difficult to precisely determine the IEC as the formal charge of OPBI is depended on pH and the percentage of crosslinking between OPBI and PVBC is unknown. Acid doping level (ADL), acid uptake (AU) and electrolyte uptake play a significant role in the conductivity of membranes in high ionic liquids.[6] Funda et al.[24] provide ADL and AU values in the supporting information for the membranes studied in the current work. It is seen that membranes containing DABCO have higher AU and ADL in all OPBI/PVBC ratios. Despite the significantly higher electrolyte uptake of the DABCO membrane,

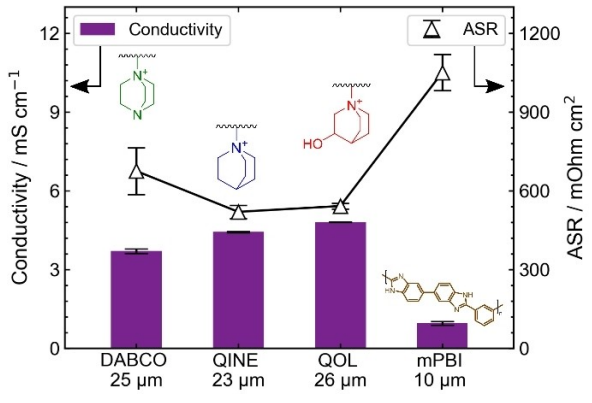

Figure 3. Conductivity (purple bars) and ASR (scatter points) determined by electrochemical impedance spectroscopy of three different 60/40 OPB-PVBC blend membranes decorated with different amine groups before any charge/discharge sequence. 10 µm mPBI is used as reference. The membrane performance was measured in a single-cell flow battery test-house under flow of an equimolar V^{+3}/V^{4+} (1.6 M total concentration of vanadium) acidic solution (2.4 M H_2SO_4).

Research Article
doi.org/10.1002/batt.202300176
Chemistry Europe
European Chemical Societies Publishing

the conductivity was similar to that of the QINE and QOL membrane. This is likely a result of the difficulty in accurately determining the thickness of a membrane when mounted in a cell. Differences in the mechanical properties of the membranes can lead to creep during compression and thus unsystematic variations in thickness. The membranes modified with DABCO may be more affected by creep deformation as they have the highest degree of electrolyte uptake and thus higher plasticization.

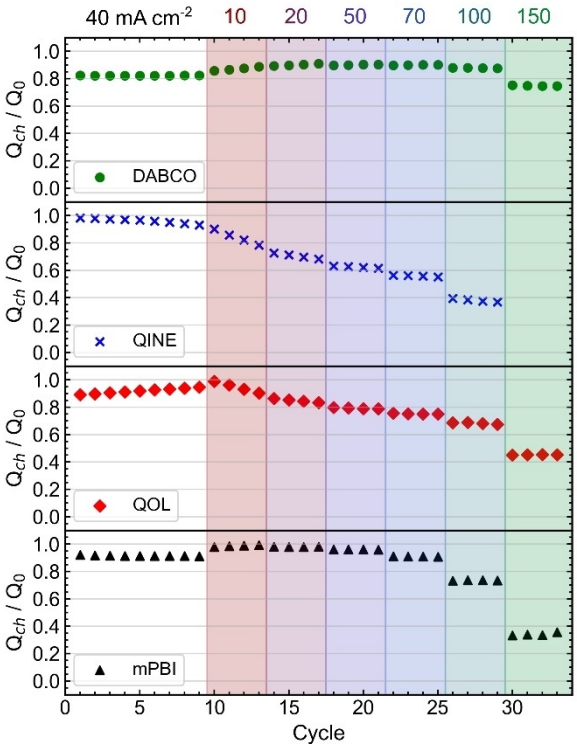

Figure 4. Capacity during charge over total capacity determined by CCCV step as a function of cycles, performed under different current densities. Cycling was performed between 0.7 V to 1.9 V under constant current. A full cycle at 10, 20, 40. 50, 70, 100, and 150 mA cm^{-2} lasted for about 15, 7, 5, 2.5, 1.5, 1, and 0.8 hours, respectively, for DABCO, mPBI and QINE. In the case of QOL the cycle time for the same current densities was 32, 15, 8, 5.5, 4, 2.5, 1 hours.

Despite the slightly higher area resistance (ASR), the DABCO-containing cell was found to outperform the cells loaded with the other membranes in terms of energy efficiency and accessible capacity during operation at all current densities tested (Figures 4 and 5). Figure 4 shows the ratio of accessible capacity during charge (Q_{ch}) over total capacity (Q_0) as a function of cycles at different current densities. The corresponding charge/discharge curves can be found in the Supporting Info, Figure S4. The total capacity was determined coulometrically by applying a constant current, constant voltage step prior to the cycles. The first 9 cycles were performed at 40 mA cm^{-2} to allow sufficient time for the membrane to equilibrate in solution. Both DABCO and mPBI showed stable performance during the first 9 cycles at 40 mA cm^{-2}. The very low capacity loss observed in conjunction with the high CE in Figure 5(A) indicates that V crossover for DABCO and mPBI is minimal. The increase in accessible capacity in QOL can be attributed to the equilibration of the membrane and the associated decrease in ohmic resistance, allowing more capacity to become accessible before reaching the potential limits. The decrease in capacity in the following four cycles at 10 mA cm^{-2} is caused by crossover, as an efficiency of 96% is measured during these cycles (Figure 5A). A similar increase of conductivity with time is seen in DABCO and mPBI. A lower capacity is recorded before reaching the potential limits in the initial 9 cycles at 40 mA cm^{-2} than in the following 4 cycles at 50 mA cm^{-2}. QINE appears to have the highest V crossover as it has the lowest CE in Figure 5(A) and the highest capacity fade at 10 mA cm^{-2} in Figure 4 (4% per cycle).

The higher voltage efficiency of DABCO in Figure 5(B), matches the expected higher transport rate in DABCO due to the higher electrolyte uptake of this membrane. It is worth noting that the cell loaded with the QINE membrane performed significantly worse compared to the other membranes and mPBI. The energy efficiency of cells with the QINE membrane was 15% to 20% lower than for cells loaded with the other membranes, at all current densities. The lack of an additional ionic group (nitrogen in DABCO and hydroxyl in QOL) significantly affects the overall performance of the membrane. The battery equipped with the QINE membrane was the only

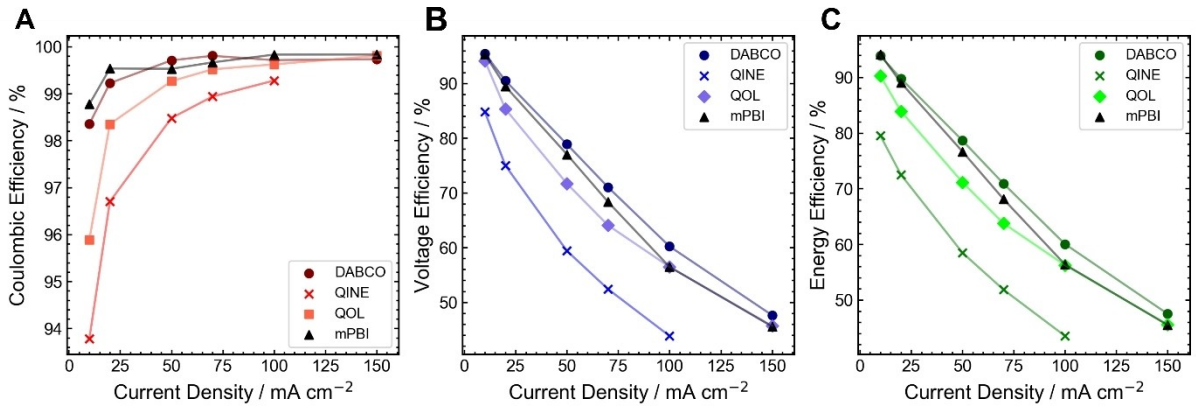

Figure 5. A) Coulombic, B) voltage and C) energy efficiency as a function of current density for the three 60/40 OBPI-PVBC blend decorated with QOL (square), DABCO (circles) and QINE (x-marks) and 10 μm mPBI (triangle)

one that could not be operated at 150 mA cm^{-2} due to the large ohmic overpotential causing the cell voltage to exceed the set potential limits (Figure 4). The other two blend membranes and untreated mPBI were operated at 150 mA cm^{-2} at a reduced capacity as the potential limits were reached more quickly due to ohmic losses (Figure 4).

It is well known that PBI exhibits excellent barrier properties for positively charged vanadium ions due to its inherent anion exchange character in acidic environment following full protonation in combination with the small polymer chain separation which effectively suppresses cross-over of the large cationic vanadium species.[11,18,22] As discussed above in connection with Figure 2, the OPBI-containing blend membranes showed very low cross-over rates in the H-cell diffusion experiment. At the device level, the coulombic efficiency provides information about the overall barrier properties of the membrane to the redox active compounds, given that no other side-reaction takes place. In operating cells, the cross-over mechanisms are complex and static diffusion measurements, which provide information about cross-over driven by diffusion, are not sufficient to fully describe the transport phenomena through the membrane that occur during cell operation.[30] At low current densities, charge/discharge cycles last longer, allowing more ions to penetrate the membrane during that time. A complete cycle at 10 mA cm^{-2} for the cells containing mPBI, DABCO and QINE lasted for about 15 h (0.13 C) while at 100 mA cm^{-2} it lasted for 1.5 h (1.3 C). For the same current densities, the cycle time for the cell containing QOL had been 32 h (0.06 C) and 2.25 h (0.8 C), respectively. At low current densities, there is more time for vanadium cations to pass through the membrane thus decreasing the CE. Side reactions such as hydrogen evolution and carbon corrosion can potentially influence the CE. However, here we assume that those side-reactions should have a constant impact on the CE across all experiments given that similar potential limits (0.7–1.9 V) are used.

In contrast, the CE above 50 mA cm^{-2} was higher than 99% in all cases except for the cell with the QINE membrane. In the static H-cell diffusion measurement, DABCO showed significantly higher cross-over as compared with QINE and QOL. The expectation was therefore to observe lower CE at low current densities for the cell equipped with DABCO compared with QINE and QOL. However, the opposite trend was observed suggesting that other transport mechanisms than diffusion dominate the vanadium cross-over through the membrane even at low current densities.

Examples of such cross-over mechanisms include pressure-driven flow, solvent diffusion, migration of redox-active species, and electroosmotic drag.[30] Pressure-driven flow and diffusion of solvent are both excluded in this case. In the former case, the pump pressure on both sides of the membranes is almost equal. In the case of the latter, no electrolyte volume change was observed during the static H-cell experiments, which lasted for 26 days that would indicate net water transport through the membrane. Migration of redox active species describes the movement of ions through the membrane driven by the applied electric field. Migration is more pronounced in membranes with high resistivity.[4,30] Among the membranes tested, 60/40 QINE showed the highest ionic resistivity based on the observed cell resistance (Figure 6, charging) and EE at high current densities. (Figure 5C, x-markers). As such, it can be assumed that migration was the main cross-over mechanism, which affected the CE, for this membrane system. Finally, electroosmotic drag describes the movement of redox-active species as the current of the primary ions (H^+, HSO_4^-) drags the solvent molecules and accompanying redox-active species.[30] As Small et al. have shown,[30] this flux is inversely proportional to the concentration of water in the membrane. Since the 60/40 DABCO membrane had a higher water uptake compared to the other two, the cross-over due to electroosmotic drag was also lower.

The cell resistance at 50% SoC determined by the slope of the potential vs the current (Figure S5, Supporting Information) is shown in Figure 6. The cell resistance is a sum of all resistance contributions in the cell, including membrane resistance, charge transfer resistance, finite diffusion resistance, distributed ohmic resistance and contact resistance.[31] The finite diffusion resistance is affected by the morphology of the electrode and the pumping rate of the electrolyte.[32] The highly porous carbon felt electrode and the high pump rate of 30 mL min^{-1} used minimizes those two losses. Contact resistance typically contributes very little to the overall cell resistance, when the electrode compression ratio is sufficiently high. The distributed ohmic resistance stem from the electrode electrolyte phase and depends on the specific ionic and electronic resistivity of the electrolyte and electrode,[32] which is similar in all experiments here given that the same type of electrodes and electrolyte were used. Charge transfer resistance may vary between tests due to different level of electrode ageing as some tests lasted longer than other did. As such, any difference seen in the cell resistance should stem from membrane and charge transfer resistance. A discrepancy can be seen between the voltage efficiency plot in Figure 5(B) and the polarization resistance in Figure 6. The cell containing QOL should have the highest voltage efficiency given the polarization resistance in Figure 6. However, DABCO has the highest voltage efficiency in all current densities. The polarization measurements were con-

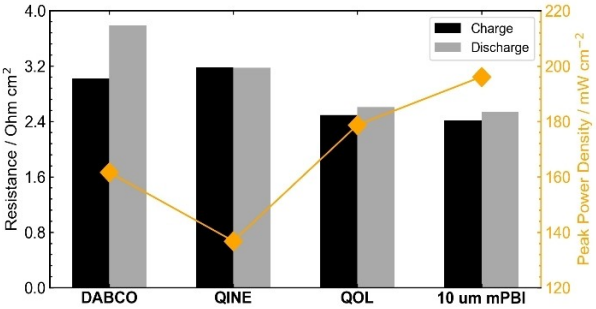

Figure 6. Cell resistance at 50% SoC of a VRFB during charge (black bar) and discharge (gray bars) with different blend membranes. These are 60/40 OPBI/PVBC blend membranes decorated with DABCO, QINE and QOL and 10 µm mPBI as a reference. The orange scatter points illustrates the peak power density at 100% SoC during discharge.

ducted after several cycles at different current densities. Ageing of the electrodes and the membranes could add to both the membrane and charge transfer resistance,[14] resulting in higher overall resistance recorded at the end of the experimental procedure.

The cells equipped with the different 60/40 blend membranes with different cationic headgroups were continuously cycled for one week. During the test, a gradual development of electrolyte imbalance occurred as indicated by liquid transfer from one side to the other. Therefore, the electrolyte was rebalanced and left to flow freely on both side with no applied potential. A non-consistent liquid transfer was observed again indicating a mechanical failure of the membrane. Visual inspection of the membranes revealed no apparent hole or damage. However, the FTIR spectra recorded prior and after electrochemical testing of the membranes showed a difference in peak intensity at 995 cm^{-1} in all DABCO, QINE and QOL (Figure S6, Supporting Information), which may originate from partial oxidation of the polymer by V^V.[3]

The cell equipped with the DABCO membrane was found to combine high coulombic, voltage, and energy efficiency during cycling, and the membrane system was selected for further testing at different blend compositions with the ambition to mitigate the electrolyte redistribution. Two other ratios were tested, with OPBI/PVBC weight ratios of 75/25 and 90/10. The FTIR spectra of the three different ratios are displayed and discussed in the Supporting Information (Figure S7).

Water and electrolyte uptake of the three DABCO blend membranes are shown in Figure 7(B). The 60/40 blend absorbed twice the amount of electrolyte compared to the other two ratios. The higher content of PVBC in the blend results in membranes capable of absorbing a higher amount of water and electrolyte. The conductivity trends follows that of water and electrolyte uptake as expected. The conductivity decreased with the increasing amount of OPBI (Figure 7A).

Interestingly, the same pattern was not observed in terms of conductivity during operation. The voltage efficiencies and subsequently energy efficiencies (Figure 9B and C) of 60/40 and 90/10 were quite similar for all current densities. The 75/25 appeared to have slightly lower voltage efficiency at most current densities other than 150 mA cm^{-2} where all three shared the same value. Similarly, the cell resistance values were close for the three membranes (Figure 8). The lowest value was observed for 30 μm thick 90/10 DABCO (2.796 Ω cm^2) followed by 24 μm 75/25 (2.881 Ω cm^2) and 28 μm 60/40 (3.020 Ω cm^2) membrane. The cell resistance of the cell with 10 μm mPBI mounted was 2.411 Ω cm^2, which is 0.385 Ω cm^2 less than of 90/10 DABCO, despite the latter being 3 times thicker. The peak power density during discharge increased as the cell resistance decreased, reaching 0.186, 0.171, 0.162 and 0.1961 W cm^{-2} for the cells equipped with the 90/10, 75/25, 60/40 and mPBI membranes, respectively. The polarization curves and the corresponding power density curves are shown in Figure S5A for 60/40 DABCO and Figure S8 for 90/10 and 75/25 DABCO.

As shown in Figure 9(A), the coulombic efficiency of the three membranes remained >98% at all current densities. The difference between the cells equipped with the different membranes was less than 1%, which may be caused by other factors aside from the blocking properties of the membranes such as electrolyte leaching or uneven flow. Charge discharge curves for the 90/10 and 75/25 DABCO can be found in the Supporting Information, Figure S9,

Contrary to 60/40 DABCO, both 75/25 and 90/10 DABCO showed no signs of electrolyte redistribution during cycling.

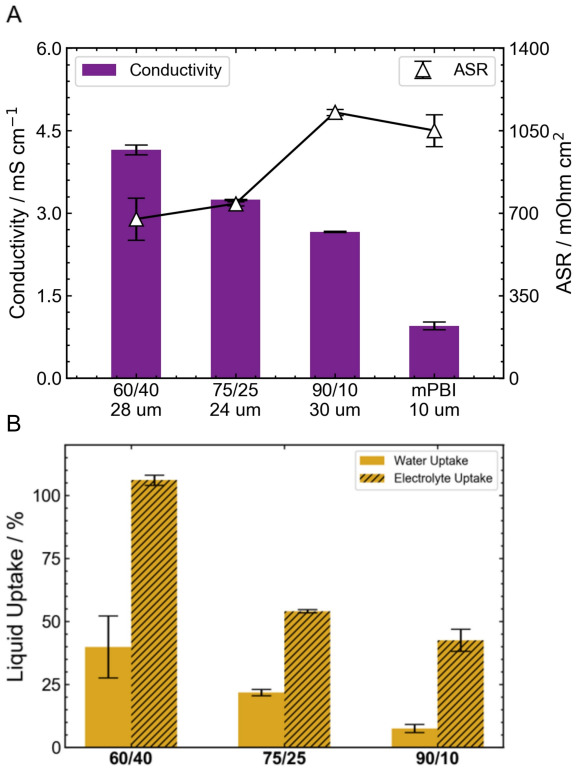

Figure 7. A) Conductivity (purple bars) and ASR (open triangles) determined by electrochemical impedance spectroscopy of blend membranes with different w/w ratios OPBI-PVBC decorated with DABCO before any charging/discharging sequence. 10 μm mPBI is used as reference. The membranes were measured under flow in a single-cell flow battery test house with an equimolar V^{+3}/V^{4+} (1.6 M total concentration of vanadium) acidic solution (2.4 M H_2SO_4) circulating. B) Water (dark yellow bars) and electrolyte (dark yellow dashed bars) absorbance of different weight ratios of OPBI/PVBC blended membranes decorated with DABCO. The electrolyte consisted of 1.6 M V^{3+} and V^{4+} dissolved in 2.4 M H_2SO_4.

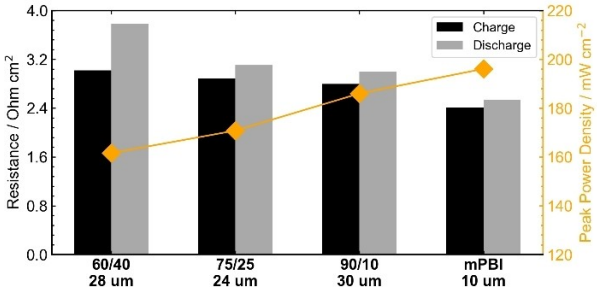

Figure 8. Cell resistance at 50% SoC of a VRFB during charge (black bar) and discharge (gray bars) with different ratios of OPBI/PVBC blend membranes decorated with DABCO. A 10 μm mPBI membrane is used as reference. The orange scatter points illustrates the peak power density at 100% SoC during discharge. The polarization curves are shown in Figure S8.

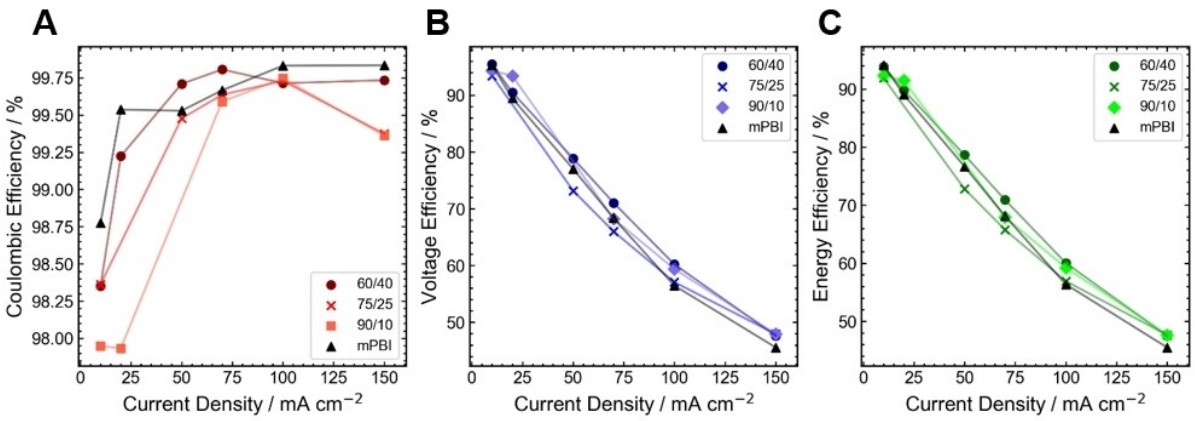

Figure 9. A) Coulombic, B) voltage and C) energy efficiency as a function of current density for 90/10 (square) 75/25 (x-marks) and 60/40 (circles) ratios of OBPI-PVBC blend decorated with DABCO. The triangles present the 10 μm mPBI used as reference.

The IR spectra of 75/25 DABCO prior and after testing showed a difference in peak intensity at 995 cm^{-1} similar to the 60/40 membranes (Figure S10). FTIR spectra of 90/10 DABCO before and after testing were similar, which indicate superior chemical stability compared to the 75/25 and 60/40 DABCO wherein a difference is seen in peak intensity at 995 cm^{-1}. The electrochemical performance of the cell with 90/10 DABCO was similar to that of the cell with the 10 μm mPBI membrane despite the former membrane being three times thicker. These results provide motivation for further modification and fabrication of thinner 90/10 DABCO membranes. Fabrication of a thinner 90/10 DABCO membrane could lead to a mechanically robust membrane that combines excellent vanadium barrier properties and high proton conductivity.

Conclusions

A series of OPBI/PVBC blend membranes decorated with three different amines, (DABCO, QOL and QINE) were fabricated and tested as separators for vanadium redox flow batteries. The $VOSO_4$ permeability of 60/40 w/w OPBI/PVBC with DABCO, QOL and QINE was very low (10^{-10} $cm^2 s^{-1}$), effectively blocking V^+ ions from crossing due to diffusion. The main crossover mechanism during battery operation was migration and electro-osmotic drag. Among the three 60/40 ratio membranes, the DABCO containing one showed the best overall performance and different OPBI/PVBC ratios with DABCO moieties membranes were tested. The other two ratios were 90/10 and 75/25 OPBI/PVBC. Electrolyte uptake was highest for the 60/40 membrane followed by 75/25 and 90/10. This was attributed to the more open structure due to higher content of PVBC. The membrane conductivity prior to testing followed the same trend. However, the overall battery performance of 90/10 exceeded both 75/25 and 60/40. The 90/10 maintained excellent stability and no sign of degradation after a week of continuous testing. The cell resistance was similar to cells with a dense mPBI despite being three times thicker. Fabricating a thinner 90/10 DABCO membrane can lead to a mechanically robust membrane with excellent barrier properties and good proton conductivity. Additionally post-modification and pre-treatment can lead to improved conductivity, while maintaining excellent blocking properties.

Supporting Information

The authors have cited additional references within the Supporting Information.[33]

Acknowledgements

This work was financially supported by Innovation Fund Denmark, Grand Solutions programme (9090-00059B, DanFlow).

Conflict of Interests

The authors declare no conflict of interest.

Data Availability Statement

The data that support the findings of this study are available from the corresponding author upon reasonable request.

Keywords: membrane · redox flow battery · PBI · vanadium redox flow battery

[1] O. Krishan, S. Suhag, *Int. J. Energy Res.* **2019**, *43*, 6171–6210.
[2] M. Zhang, M. Moore, J. S. Watson, T. A. Zawodzinski, R. M. Counce, **2012**, 10.1149/2.041208jes.
[3] X. Z. Yuan, C. Song, A. Platt, N. Zhao, H. Wang, H. Li, K. Fatih, D. Jang, *Int. J. Energy Res.* **2019**, *43*, 6599–6638.
[4] S. Bukola, A. Vise, Y. Li, G. Goenaga, T. A. Zawodzinski, J. L. Blackburn, B. Pivovar, *ACS Appl. Polym. Mater.* **2022**, *4*, 381–393.
[5] P. C. Ghimire, A. Bhattarai, T. M. Lim, N. Wai, M. Skyllas-kazacos, Q. Yan, *Batteries* **2021**, 1–36.

[6] K. D. Kreuer, A. Münchinger, *Annu. Rev. Mater. Res.* **2021**, *51*, 21–46.
[7] J. K. Jang, S. W. Jo, J. W. Jeon, B. G. Kim, S. J. Yoon, D. M. Yu, Y. T. Hong, H. T. Kim, T. H. Kim, *ACS Appl. Energ. Mater.* **2021**, *4*, 4672–4685.
[8] T. Wang, J. Han, K. Kim, A. Münchinger, Y. Gao, A. Farchi, Y. K. Choe, K. D. Kreuer, C. Bae, S. Kim, *Mater Adv* **2020**, *1*, 2206–2218.
[9] T.-S. Chung, *Polym. Rev.* **1997**, *37*, 277–301.
[10] D. Aili, J. Yang, K. Jankova, D. Henkensmeier, Q. Li, *J. Mater. Chem. A* **2020**, *8*, 12854–12886.
[11] C. Noh, M. Jung, D. Henkensmeier, S. W. Nam, Y. Kwon, *ACS Appl. Mater. Interfaces* **2017**, *9*, 36799–36809.
[12] M. Di, L. Hu, L. Gao, X. Yan, W. Zheng, Y. Dai, X. Jiang, X. Wu, G. He, *Chem. Eng. J.* **2020**, *399*, 125833.
[13] L. Ding, Y. Wang, L. Wang, Z. Zhao, M. He, Y. Song, *J. Power Sources* **2020**, *455*, 227965.
[14] M. Mara Ikhsan, S. Abbas, X. H. Do, S. Y. Choi, K. Azizi, H. A. Hjuler, J. H. Jang, H. Y. Ha, D. Henkensmeier, *Chem. Eng. J.* **2022**, *435*, 134902.
[15] J. C. Duburg, K. Azizi, S. Primdahl, H. A. Hjuler, E. Zanzola, T. J. Schmidt, L. Gubler, *Molecules* **2021**, *26*, 26061679.
[16] L. Gubler, D. Vonlanthen, A. Schneider, *J. Electrochem. Soc.* **2020**, *167*, 100502.
[17] I. Strużyńska-Piron, M. Jung, A. Maljusch, O. Conradi, S. Kim, J. H. Jang, H. J. Kim, Y. Kwon, S. W. Nam, D. Henkensmeier, *Eur. Polym. J.* **2017**, *96*, 383–392.
[18] M. Jung, W. Lee, N. Nambi Krishnan, S. Kim, G. Gupta, L. Komsiyska, C. Harms, Y. Kwon, D. Henkensmeier, *Appl. Surf. Sci.* **2018**, *450*, 301–311.
[19] X. Yan, Z. Dong, M. Di, L. Hu, C. Zhang, Y. Pan, N. Zhang, X. Jiang, X. Wu, J. Wang, G. He, *J. Membr. Sci.* **2020**, *596*, 117616.
[20] Z. Dong, M. Di, L. Hu, L. Gao, X. Yan, X. Ruan, X. Wu, G. He, *J. Membr. Sci.* **2020**, *608*, 118179.
[21] X. Ren, L. Zhao, X. Che, Y. Cai, Y. Li, H. Li, H. Chen, H. He, J. Liu, J. Yang, *J. Power Sources* **2020**, *457*, 228037.
[22] Y. Chen, P. Xiong, S. Xiao, Y. Zhu, S. Peng, G. He, *Energy Storage Mater.* **2022**, *45*, 595–617.
[23] D. Chen, X. Chen, L. Ding, X. Li, *J. Membr. Sci.* **2018**, *553*, 25–31.
[24] F. Arslan, K. Chuluunbandi, A. T. S. Freiberg, A. Kormanyos, F. Sit, S. Cherevko, J. Kerres, S. Thiele, T. Böhm, *ACS Appl. Mater. Interfaces* **2021**, *13*, 56584–56596.
[25] H. Li, M. R. Kraglund, A. K. Reumert, X. Ren, D. Aili, J. Yang, *J. Mater. Chem. A* **2019**, *7*, 17914–17922.
[26] H. Li, N. Yu, F. Gellrich, A. K. Reumert, M. R. Kraglund, J. Dong, D. Aili, J. Yang, *J. Membr. Sci.* **2021**, *633*, 10.1016/j.memsci.2021.119418.
[27] V. K. Aggarwal, I. Emme, S. Y. Fulford, *J. Org. Chem.* **2003**, *68*, 692–700.
[28] R. E. Coppola, D. Herranz, R. Escudero-Cid, N. Ming, N. B. D'Accorso, P. Ocón, G. C. Abuin, *Renewable Energy* **2020**, *157*, 71–82.
[29] M. A. Aziz, S. Shanmugam, *J. Mater. Chem. A* **2017**, *5*, 16663–16671.
[30] L. J. Small, H. D. Pratt, T. M. Anderson, *J. Electrochem. Soc.* **2019**, *166*, A2536–A2542.
[31] C.-N. Sun, F. M. Delnick, D. S. Aaron, A. B. Papandrew, M. M. Mench, T. A. Zawodzinski, *J. Electrochem. Soc.* **2014**, *161*, A981–A988.
[32] A. M. Pezeshki, R. L. Sacci, F. M. Delnick, D. S. Aaron, M. M. Mench, *Electrochim. Acta* **2017**, *229*, 261–270.
[33] T. Ou, H. Chen, B. Hu, H. Zheng, W. Li, Y. Wang, *Int. J. Hydrogen Energy* **2018**, *43*, 12337–12345.

Manuscript received: April 25, 2023
Revised manuscript received: July 11, 2023
Version of record online: July 31, 2023